Journal of Natural Gas Science and Engineering 59 (2018) 21–34

Contents lists available at ScienceDirect

Journal of Natural Gas Science and Engineering

journal homepage: www.elsevier.com/locate/jngse

# The role of fault gouge properties on fault reactivation during hydraulic stimulation; an experimental study using analogue faults

A.C. Wiseall*, R.J. Cuss, E. Hough, S.J. Kemp

*British Geological Survey, Kingsley Dunham Centre, Nicker Hill, Keyworth, Nottingham, UK*

ARTICLE INFO

*Keywords:*
Shale gas
Bowland shale
Fault reactivation
Hydraulic fracturing
Fractures

ABSTRACT

During the hydraulic stimulation of shale gas reservoirs the pore pressure on pre-existing faults/fractures can be raised sufficiently to cause reactivation/slip. There is some discrepancy in the literature over whether this interaction is beneficial or not to hydrocarbon extraction. Some state that the interaction will enhance the connectivity of fractures and also increase the Stimulated Reservoir Volume. However, other research states that natural fractures may cause leak-off of fracturing fluid away from the target zone, therefore reducing the amount of hydrocarbons extracted. Furthermore, at a larger scale there is potential for the reactivation of larger faults, this has the potential to harm the well integrity or cause leakage of fracturing fluid to overlying aquifers.

In order to understand fault reactivation potential during hydraulic stimulation a series of analogue tests have been performed. These tests were conducted using a Bowland Shale gouge in the Angled Shear Rig (ASR). Firstly, the gouge was sheared until critically stressed. Water was then injected into the gouge to simulate pore fluid increase as a response to hydraulic stimulation. A number of experimental parameters were monitored to identify fracture reactivation. This study examined the effect of stress state, moisture content, and mineralogy on the fault properties.

The mechanical strength of a gouge increases with stress and therefore depth. As expected, a reduction of moisture content also resulted in a small increase in mechanical strength. Results were compared with tests previously performed using the ASR apparatus, these showed that mineralogy will also affect the mechanical strength of the gouge. However, further work is required to investigate the roles of specific minerals, e.g. quartz content. During the reactivation phase of testing all tests reactivated, releasing small amounts of energy. This indicates that in these basic conditions natural fractures and faults will reactivate during the hydraulic stimulation if critically stressed. Furthermore, more variables should be investigated in the future, such as the effect of fluid injection rate and type of fluid.

## 1. Introduction

The extraction of natural gas and oil from unconventional shale source rocks has become a key onshore energy source (Arthur et al., 2008). In 2014 approximately 48% of the total U.S dry natural gas was produced by this method, with that number predicted to rise to 69% by 2040 (EIA, 2016). The European Union Energy Roadmap 2050 forecasts a similar trend in natural gas production from unconventional reservoirs in Europe (EU, 2011). Shale gas is a critical energy source as Europe transitions from coal-powered electricity generation to a more environmentally friendly energy mix. However, the hydraulic fracturing technique associated with shale gas production has geological, engineering and environmental challenges and concerns associated with it. These need to be overcome to create an efficient, cleaner, and socially acceptable shale gas industry in Europe.

Hydraulic fracturing involves drilling a deviated well within a shale formation at depths of up to 5 km (Geol.Soc., 2013). The deviated well is perforated within the target area and high pressure fluid is injected into the formation to create a fracture network with enhanced permeability. The fluid is pumped in at a pressure that overcomes the tensile strength of the shale, thus producing a hydraulic fracture network. Several overviews of the hydraulic fracturing process are available in the literature (e.g. API, 2009; Cuss et al., 2015; Mair et al., 2012). Shale is a naturally heterogeneous rock and can contain many discontinuities (fractures, faults, joints, bedding planes) at a range of scales (e.g. Ougier-Simonin et al., 2016; Gale et al., 2014). Therefore, during the hydraulic fracturing process it is likely that the man-made fracture network will interact with naturally occurring discontinuities within

* Corresponding author.
*E-mail address:* andyw@bgs.ac.uk (A.C. Wiseall).

https://doi.org/10.1016/j.jngse.2018.08.021
Received 20 June 2018; Received in revised form 31 July 2018; Accepted 21 August 2018
Available online 27 August 2018

the shale. The interaction of fracture networks is a key area of research identified by a number of studies (Fisher and Warpinski, 2012; Arthur et al., 2008; Cuss et al., 2015; Rutqvist et al., 2013; Davies et al., 2012). There is disagreement over whether the interaction of man-made fractures with natural fractures will enhance hydrocarbon recovery or not (Gale et al., 2007; Montgomery et al., 2005). The area over which the hydraulic fracture network is produced is commonly referred to as the Stimulated Reservoir Volume (SRV). It is generally assumed that the larger the SRV the higher the volume of hydrocarbons extracted. The SRV could be enhanced by the interaction with natural fractures, resulting in more hydrocarbons being produced. However, some studies indicate that natural fractures lead to the fracturing fluid flowing away from the target area and therefore reducing the impact of the hydraulic fracturing process.

Injection of pore fluids at an elevated magnitude compared with in situ pore pressure can result in changes of in situ conditions; this is likely to be manifest as a change in pore pressure within the reservoir. This perturbation, if sufficient in magnitude, may result in the reactivation of pre-existing fault systems that are close to the point of failure. It is believed that hydraulic stimulation at the Preese Hall site in Lancashire UK, resulted in the reactivation of a large, previously unidentified fault (Clarke et al., 2014). Two seismic events, of a magnitude $M_L = 2.3$ and 1.5 on the Richter scale were observed. These relatively small seismic events were attributed to the injection of fracturing fluid onto the fault zone (De Pater and Baisch, 2011). It must be noted that these can be considered relatively large when discussing shale gas exploitation. The majority of seismic events associated with production of the Barnett Shale in the US are typically less than $M_L = 1$ (Maxwell et al., 2006); therefore the detected events at Preese Hall are considered to be relatively large. Earthquakes of this magnitude as experienced at Preese Hall have the potential to damage well integrity and have the potential to result in leakage of fracturing fluid into shallow aquifers through loss of well integrity. It is therefore important to understand the role of hydraulic stimulation on fault reactivation/fracture slip. It should be noted that during this study the terms 'fracture' and 'fault' will be used interchangeably with the assumption of the observations will be observed over a range of scales.

Complex hydro-mechanical interactions occur during the hydraulic fracturing process. The injection of the fracturing fluid into the unconventional reservoir locally raises the pore pressure. This results in a reduction of effective stress as pore pressure acts in the opposing direction to confining stress (Terzaghi, 1943):

$$\sigma' = \sigma - u \quad [1]$$

where $u$ is pore pressure, $\sigma$ is confining stress and $\sigma'$ is effective stress. Hubbert and Rubbey (1959) recognised that this theory applies to faults. The increase in pore pressure and resultant reduction in effective stress on a fault can lead to reactivation, as illustrated by Equation (2). The increase in pore pressure from the injection of the hydraulic fracturing fluid therefore has the potential to cause reactivation of natural pre-existing faults. The point at which reactivation will occur can be defined by the Mohr-Coulomb failure criterion:

$$\tau_f = C + \mu\sigma_n' = C + \mu(\sigma_n - u) \quad [2]$$

where $C$ is cohesive strength of the fault, $\mu$ is coefficient of friction, $\sigma_n$ is normal stress on the fault, $u$ is pore pressure and $\sigma_n'$ denotes effective normal stress. Therefore, an increase in pore pressure may result in the loss of frictional strength on a pre-existing discontinuity (fracture, fault, joint etc.), resulting in movement along that discontinuity.

In order to define the potential for reactivation within a potential shale formation a number of characteristics must be defined. As can be seen in Fig. 1, the angle of the fault ($\theta$) with respect to the stress field determines if the fault is critically stressed and therefore prone to reactivation. The material within the fracture, often referred to as the gouge, is also an important control on the potential for reactivation. Gale et al. (2014) review many of the natural fractures found within the major US shale formations. Many were filled with calcite, although some quartz-filled fractures were observed. Montgomery et al. (2005) regard calcite-filled fractures as barriers to fluid flow. However, Gale et al. (2007) oppose this view and argue the low tensile strength of the cement in comparison to the protolith means that reactivation will occur and therefore not act as a barrier to fluid flow. Gale and Holder (2008) also showed that calcite filled fractures have half the strength of intact rock. These contrasting views highlight the importance of understanding the effect that the fracture gouge can have on the hydro-mechanical properties of the fault and the potential for reactivation.

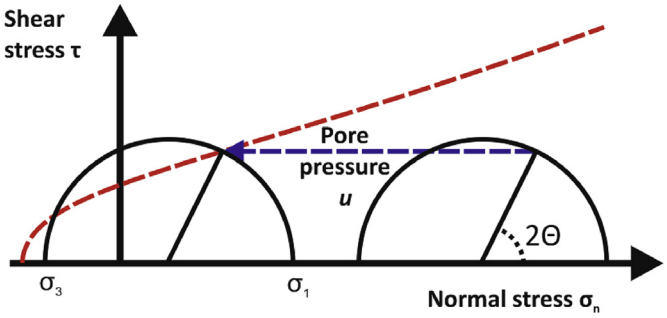


**Fig. 1.** Mohr circle diagram showing the stress state of a fault and the subsequent effect of an increase in pore pressure (u). The fault is orientated at 2θ and becomes critically stressed once it crosses the failure envelope (dashed line).

Another controlling factor on reactivation potential is the water content of the gouge. Water content, or degree of saturation, has been shown to have a specific weakening effect on rock strength when compared with dry conditions (Paterson, 1978). This behaviour has been observed in many laboratory tests, e.g. uniaxial, triaxial and hydrostatic deformation testing (Dyke and Dobereiner, 1991; Hawkins and McConnel, 1992; Serdengecti and Boozer, 1961; Rutter, 1972; Zhu and Wong, 1997). However, many of these tests were conducted on common reservoir and aquifer rocks such as sandstones (Cuss, 1999; Boozer et al., 1963). Thus meaning there is paucity in data describing the effect of saturation on shale strength. A study by Ikari et al. (2007) showed that moisture content can have a significant effect on the mechanical properties of faults. Therefore, it is important to understand how varying moisture content could effect the potential for fault reactivation in natural discontinuities within shale.

This study presents results from a series of analogue tests carried out with the aim of simulating reactivation of a critically stressed fault/fracture through increases in pore fluid pressure as a result of hydraulic stimulation. The Bowland Shale has been highlighted as a potential shale resource formation in northern England. Previous analogue studies have used the same methodology and demonstrated that mineralogy has an effect on both the mechanical properties of faults and fault reactivation (Cuss and Harrington, 2016; Cuss et al., 2016). The current study aimed to advance previously studies and apply observations to the shale gas industry. The main objectives of the study were to investigate:

- mechanical properties of a Bowland Shale filled fault gouge;
- reactivation potential of a Bowland Shale filled fault gouge;
- effect of moisture content on the mechanical properties and reactivation potential of the fault gouge.

These objectives were achieved through a series of analogue fault gouge experiments. The analogue tests would recreate a basic fault system with the ability to increase the pore pressure on the fault. This would therefore simulate pore pressure perturbations as a result of hydraulic stimulation and provide information relevant to fault strength and fault reactivation potential within an unconventional reservoir.

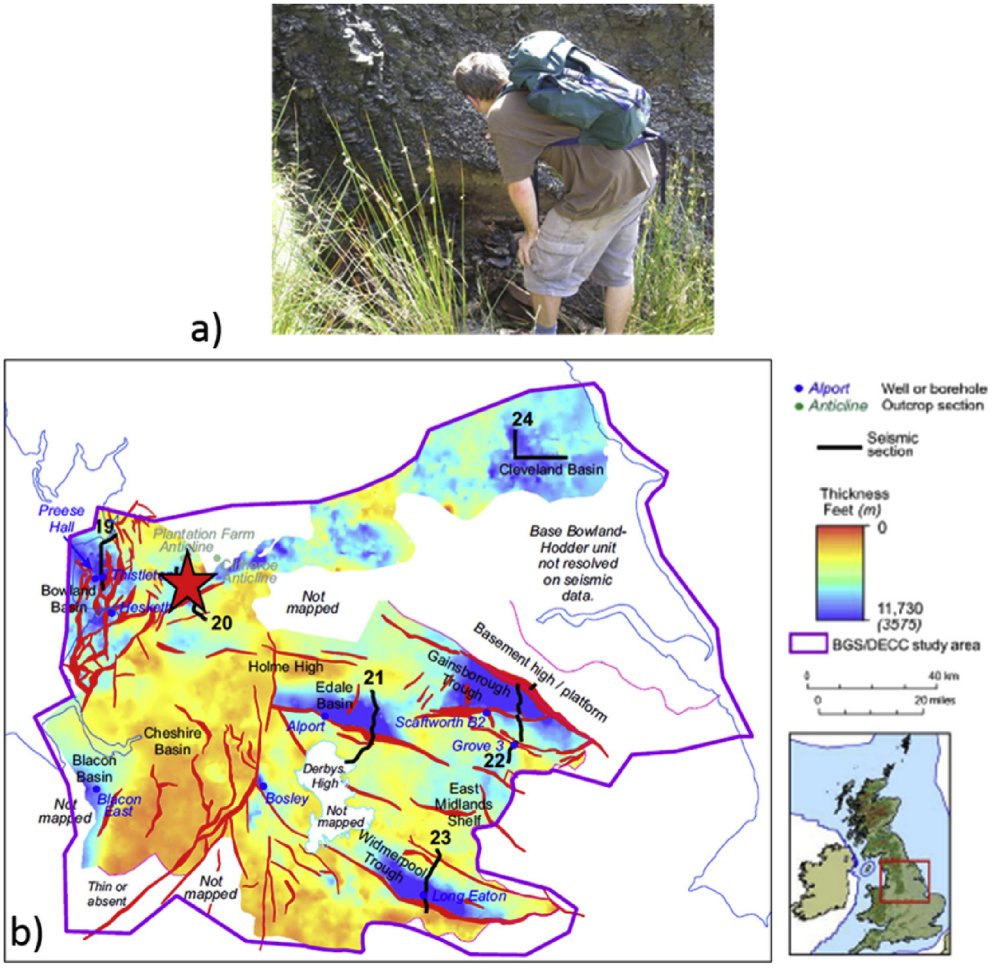


**Fig. 2.** (a) photo showing samples being collected from an exposed streambed at Parlick Hill, north-west England, (b) map showing thickness of the Bowland Shale in northern England, the star shows the location of the Pennine Basin. After Andrews (2013).

## 2. Testing methodology

### 2.1. Tested material

The Bowland Shale is mid Carboniferous in age (Serpukhovian, upper Mississippian) and accumulated in the Pennine Basin, which underlies much of northern England. Borehole material of this stratigraphic unit is limited to core that is typically desiccated, sub-sampled and slabbed rendering it unsuitable for many engineering tests. As a result a suitable sized block of fresh outcrop material was used. The low strength of mud-prone units results in outcrop generally being restricted to better-cemented calcareous intervals. These will have been subject to weathering processes and therefore may not be fully representative of the material at depth. The Bowland Shale and slightly older Hodder Mudstones have been identified as the principal shale gas resource in the UK (Andrews, 2013), although there is little exploration data to confirm the likely reserve. Samples from the upper part of the Bowland Shale were selected for this study from the north-western part of the Pennine Basin (Fig. 2a). A suitable outcrop was identified in a small natural stream section at Parlick Hill in central Lancashire (53°54′01.34″ N, 2°37′35.78″W) (Fig. 2b). The outcrop is located in the central part of the Upper Bowland Shale, approximately 100 m above the base and 65 m below the Tumulites pseudobilinguis ($E_{1b}2$) local ammonoid marker horizon. The mudstone was deposited in a deep water setting, and is typical of the carbonate-rich 'offshore muds' facies as described by Andrews (2013) and 'calcareous mudstones' of Konitzer et al. (2014).

The collected material was ball milled to form a powder with a grain size of ≤53 μm. The resulting powder was mixed with de-ionised water to form a saturated paste; this represented the tested fault gouge. X-ray diffraction (XRD) analysis was performed on the powder giving bulk mineralogy and the mineralogy of grains under 2 μm. These results are

**Table 1**
XRD analysis showing the bulk mineralogy and clay sized particles of the gouge.

| Mineral (wt%) | | | | | | | | | | Proportion of clay minerals in < 2 μm fraction (%) | | | | I/S species | Non clays |
|---|---|---|---|---|---|---|---|---|---|---|---|---|---|---|---|
| Silicates | | | Carbonates | | Clay minerals | | | Sulphide and phosphate | | | | | | | |
| quartz | K-feldspar | plagioclase | calcite | dolomite | 'mica' | kaolinite | chlorite | pyrite | apatite | illite | chlorite | kaolinite | I/S | | |
| 24.1 | 1.1 | < 0.5 | 33.0 | 15.5 | 18.2 | 3.1 | 0.6 | 2.3 | 2.0 | 48 | 4 | 9 | 39 | 80%I, R1 | qtz, plag, pyrite |

presented in Table 1.

### 2.2. Apparatus

The experiments were performed using the Angled Shear Rig (ASR), which was designed and built at the British Geological Survey. The ASR consists of five constituent parts:

1. A rigid steel body chosen as it has bulk modulus of compressibility and shear modulus approximately two orders of magnitude greater than any clay gouge tested. Therefore, the apparatus is not likely to undergo any noticeable deformation during testing;
2. Vertical load was provided by an Enerpac hydraulic ram that was linked to a Teledyne/ISCO 260D syringe pump for control. The ram provided force to a rigid loading frame and an upper thrust block. This system was capable of providing a vertical stress of up to 20 MPa. The Enerpac ram had a stroke of 105 mm, this meant that there was sufficient stroke to accommodate the vertical movement of the top block during shearing;
3. Shear was provided by a shear force actuator, this consisted of an modified and horizontally mounted Teledyne/ISCO 500D syringe pump. This could provide a shear rate as low as 14 microns a day or as fast as 0.5 mm per second;
4. Pore pressure system comprising a Teledyne/ISCO 500D syringe pump that could deliver fluid up to a pressure of 25.8 MPa. The syringe pump delivered water through the centre of the top block directly to the fault surface;
5. A bespoke designed data acquisition system using National Instruments LabView™ software. This provided the ability to control and monitor all test parameters. All data channels were logged every 60 s.

Fig. 3 shows the experimental assembly of the ASR. The top and bottom block, which created the angled fracture surface, were made up of 316 stainless steel and arranged to give a dip of 30° with respect to the shear direction. The faces of the two blocks were polished so not to introduce any preferential pathways for fluid flow. The vertical load was provided to the fault surface by a syringe pump and hydraulic ram, however it should be noted that the vertical load provided by the syringe pump did not equate to the normal load. The top block also consisted a central injection port and two orthogonally arranged pore pressure sensors. The top block was 60 × 60 mm, meaning that the gouge had a top and bottom area of this size.

The shearing force for the ASR was provided by the shear force actuator, this moved the bottom block creating a slip-plane between the two blocks. The movement of the bottom block was measured using a linear variable differential transducer (LVDT), which had a full range of ± 25 mm and an accuracy of 0.5 µm. The vertical movement of the top block was measured by two non-contact eddy current sensors, which had a full range of ± 0.5 mm and an accuracy of 0.06 µm.

The tests in this study were all performed using a gouge made up of Bowland Shale. The ball-milled shale was mixed with de-ionised water to form a paste. This study aimed to research the effect of moisture content on fault properties and therefore two sets of tests at differing moisture content were carried out; a fully saturated set and a partially saturated set. The fully saturated fault gouges consisted of 35 g of Bowland Shale powder and 15 g of de-ionised water; the partially saturated gouges used 35 g of powder and 12.5 g of de-ionised water. In both cases the powder and water were mixed together for 5 min by a combination of hand and blender to form a homogeneous fault gouge material. The paste was placed by hand onto the polished surface of the top block, this was slowly lowered onto the angled plane with care not deform the paste. A vertical load was applied to the gouge, the tests were performed at vertical stress ranging from 1 MPa to 6.25 MPa in 1.3 MPa steps, as shown in Table 2. The gouge was not laterally confined as sealing elements would be needed at the exteriors of the top block. These would introduce an unwanted frictional component that is likely to have overshadowed the low frictional properties of the clay. Previous tests on this apparatus have shown the gouge thickness to be approximately 180 µm (Cuss et al., 2018), which is greater than the maximum grain size of 53 µm and therefore the gouge was not compressed to be a mono-layer of clay and water.

The testing phase can be divided into two parts; a shearing phase and an injection phase. During the shearing phase, the vertical load was maintained constant and the shear actuator created a constant rate displacement of 1 mm over a 24-h period. This was a sufficient period for the gouge to reach yield and peak shear stress conditions. Once this had been achieved the shearing phase ended and the injection phase began. De-ionised water was injected through the top block into the gouge at a constant injection rate of 100 µl $h^{-1}$. As a result, pore pressure in the gouge increased. Slip was identified as a simultaneous drop in the shear stress and/or a change in the vertical displacement.

#### 2.2.1. Test scenario

The current study simulated a change in pore pressure on a pre-existing critically stressed fracture/fault as the result of hydraulic stimulation. Analogue tests were used to investigate the influence of certain parameters on the gouge properties. The use of the analogue arrangement meant that tests could be repeated under near-identical conditions and therefore allow the influence of moisture content on the reactivation potential to be investigated. Fracture roughness has been shown to effect the hydro-mechanical properties of a fault (e.g. Cuss et al., 2009, 2011). However, a smooth analogue fracture plane was used in this study to reduce the number of tested variables and allow tests to be repeated under identical conditions. Shear or fracturing tests could have been conducted on intact samples. However, this introduces extra variables that affect test repeatability, e.g. fracture roughness. Therefore, the testing arrangement allowed isolation of variability associated with moisture content on slip potential. It should be noted that tests were conducted up to a maximum vertical stress of 6.2 MPa. These

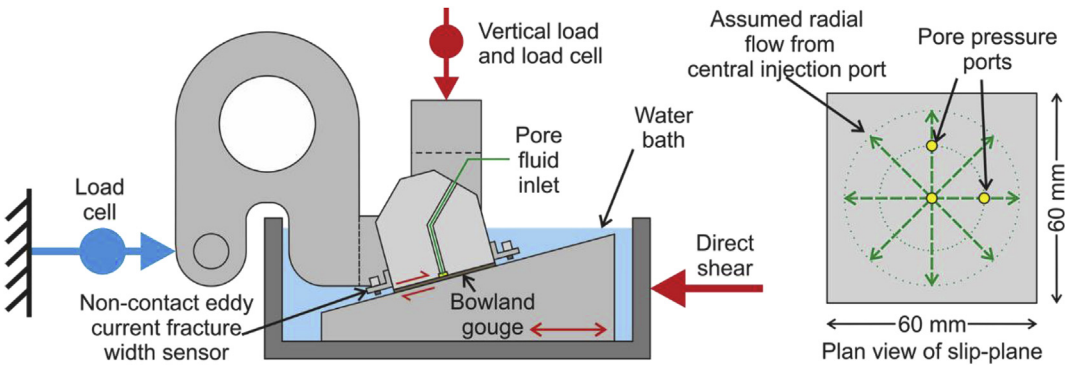


**Fig. 3.** Schematic of the angled shear rig.

**Table 2**
Mechanical and reactivation data.

| Test number | Moisture state | Pump pressure | Average vertical stress | Starting shear stress | Yield stress | Maximum shear stress | Reactivation pressure | Vertical stress on reactivation | Shear stress on reactivation | Q on reactivation | P on reactivation | Number of reactivations | Shear modulus |
|---|---|---|---|---|---|---|---|---|---|---|---|---|---|
| | | (MPa) | (MPa) | (MPa) | (MPa) | (MPa) | (MPa) | (MPa) | (MPa) | (MPa) | (MPa) | | (MPa) |
| 5 | HM | 2.5 | 1.07 | 0.29 | 0.91 | 0.93 | 0.17 | 1.08 | 0.90 | 0.18 | 0.79 | 3 | 120 |
| 3 | HM | 5 | 2.59 | 0.66 | 2.20 | 2.26 | 0.28 | 2.50 | 2.19 | 0.31 | 2.01 | 7 | 231 |
| 2 | HM | 7.5 | 3.78 | 0.99 | 3.21 | 3.35 | 0.36 | 3.84 | 3.27 | 0.57 | 3.10 | 5 | 345 |
| 4 | HM | 10 | 4.98 | 1.19 | 3.99 | 4.56 | 0.83 | 5.05 | 4.45 | 0.60 | 3.81 | 8 | 294 |
| 6 | HM | 12.5 | 6.24 | 1.52 | 5.25 | 5.46 | 1.27 | 6.30 | 5.28 | 1.02 | 4.36 | 4 | 428 |
| 16 | LM | 2.5 | 1.37 | 0.38 | 1.42 | 1.43 | 0.17 | 1.38 | 1.33 | 0.05 | 1.17 | 4 | 402 |
| 10 | LM | 5 | 2.54 | 0.82 | 2.11 | 2.15 | 0.58 | 2.54 | 2.07 | 0.54 | 1.67 | 6 | 150 |
| 8 | LM | 7.5 | 3.78 | 1.34 | 3.07 | 3.87 | 0.89 | 3.85 | 3.11 | 0.74 | 2.47 | 2 | 259 |
| 14 | LM | 10 | 4.96 | 1.60 | 4.19 | 4.24 | 1.29 | 5.03 | 4.08 | 0.96 | 3.11 | 4 | 886 |
| 11 | LM | 12.5 | 6.23 | 2.16 | 5.20 | 5.74 | 2.06 | 6.23 | 5.55 | 0.69 | 3.71 | 2 | 666 |

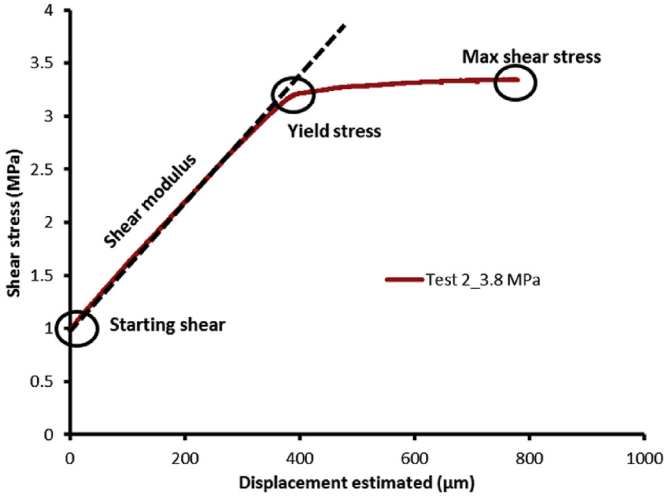


**Fig. 4.** Results of Test 2_3.8 MPa. Typical shear stress and displacement curve showing the mechanical properties measured, i.e. starting shear stress, yield stress, and maximum shear stress.

are relatively low stresses considering hydraulic stimulation is likely to occur at depths greater than 1.5 km (Geol soc., 2013) where the vertical stress is likely to be approximately 34.5 MPa and effective stress will be 19.5 MPa (23 MPa $km^{-1}$ from Zoback, 2010).

## 3. Results

The results of ten experiments are reported in this study. As discussed above, each experiment had a shearing phase and an injection phase. The purpose of the shearing phase was to take the gouge beyond yield and into a critically stressed state. Fig. 4 shows the results of Test 2_3.8 MPa. This is a typical shear stress response observed during these tests. Highlighted are the starting shear stress, yield stress and the maximum shear stress, as well as the shear modulus being the gradient of the linear portion of the graph. These are the main values recorded during the shearing phase.

Fig. 5 presents the results of the shearing phase for each of the ten tests conducted. Fig. 5a shows the results of the tests performed on the fully saturated gouge, whereas Fig. 5b shows the results of the partially saturated gouge. Table 2 gives the mechanical data for each of the tests.

Fig. 5a shows that the starting shear stress for each test increased with the increasing vertical stress on the fault. All tests in Fig. 5a showed an initial linear response as the gouge was sheared, this ends when the gouge reached the yield stress. The yield stress increased from 0.91 MPa in the lowest vertical stress state to 5.25 MPa in the highest vertical stress case. There is a relatively consistent increase in yield between each test as the vertical stress increased. As well as the yield increasing with stress, so did the shear modulus, increasing from 120 MPa to 428 MPa. However, between Test 2 and 4, the vertical stress increased from 3.78 MPa to 4.98 MPa but the shear modulus decreased from 345 to 294 MPa; this was not expected. Once the gouge reached yield the shear stress no longer increased at the same rate. In Tests 2,3,5 the shear stress only slightly increased after yield. However, in Test 4 the shear stress continued increasing but at a much lower rate. In Test 6 a small drop in shear stress could be observed and the shear stress subsequently increased slowly. The maximum shear stress recorded in each test ranged from 0.93 to 5.45 MPa with the increasing vertical stress.

Fig. 5b shows the results from the shearing phase of testing on the partially saturated gouge. As can be seen the results have a more complex mechanical response. For instance, Test 14 at 5 MPa vertical stress had a lower starting shear stress than Test 8 at 3.8 MPa, which was contrary to the trend seen in the fully saturated tests. This may

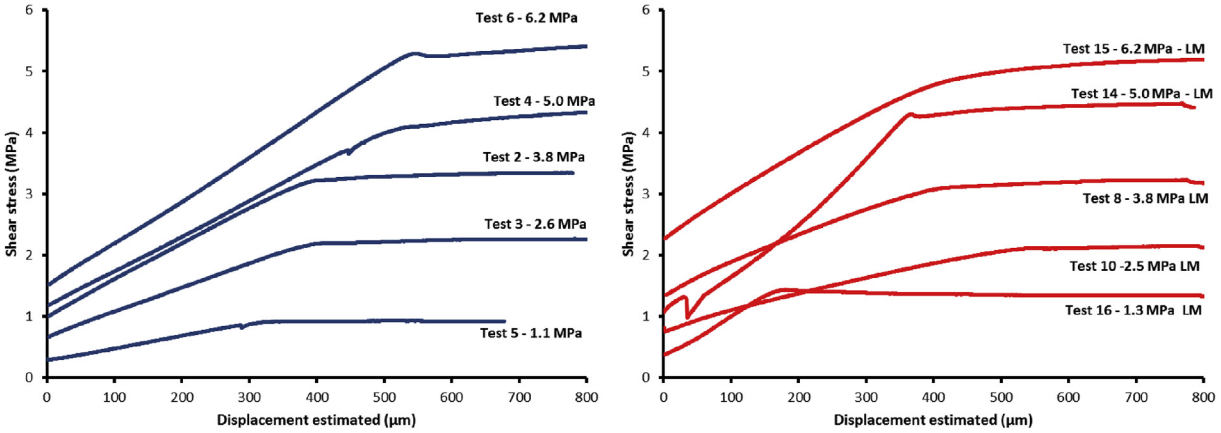


**Fig. 5.** Results of phase one of the experimental study. (a) shear-displacement response of fully saturated gouge, (b) shear displacement response of the partially saturated gouge, LM = Lower moisture content. The Test number and vertical stress applied to the gouge are shown for each test.

have been as a result of gouge shearing during setup of the experiment. Test 14 had a different mechanical response to the majority of the tests carried out with the partially saturated gouge. The shear modulus was much greater for this test compared with Tests 8, 10 and 15. Test 14 also had a large drop in shear stress towards the start of the shearing phase. Test 16 also had a higher shear modulus than Test 10. However, the yield stress for all tests increased with vertical stress, as did peak shear stress. As with the higher moisture content tests, the majority of the tests show a response which could be described as elastoplastic deformation.

In Fig. 6 we compare the mechanical data (starting shear stress, yield, and maximum shear stress). This allows direct comparisons to be drawn between the two sets of tests performed at different moisture content. Fig. 6a and b both show a linear relationship between the starting shear stress and vertical stress on the gouge. The same can be observed for both the yield and maximum shear stress data for both gouge saturation states. Fig. 6c allows a direction comparison of results from the two sets of tests performed. The lower moisture content tests

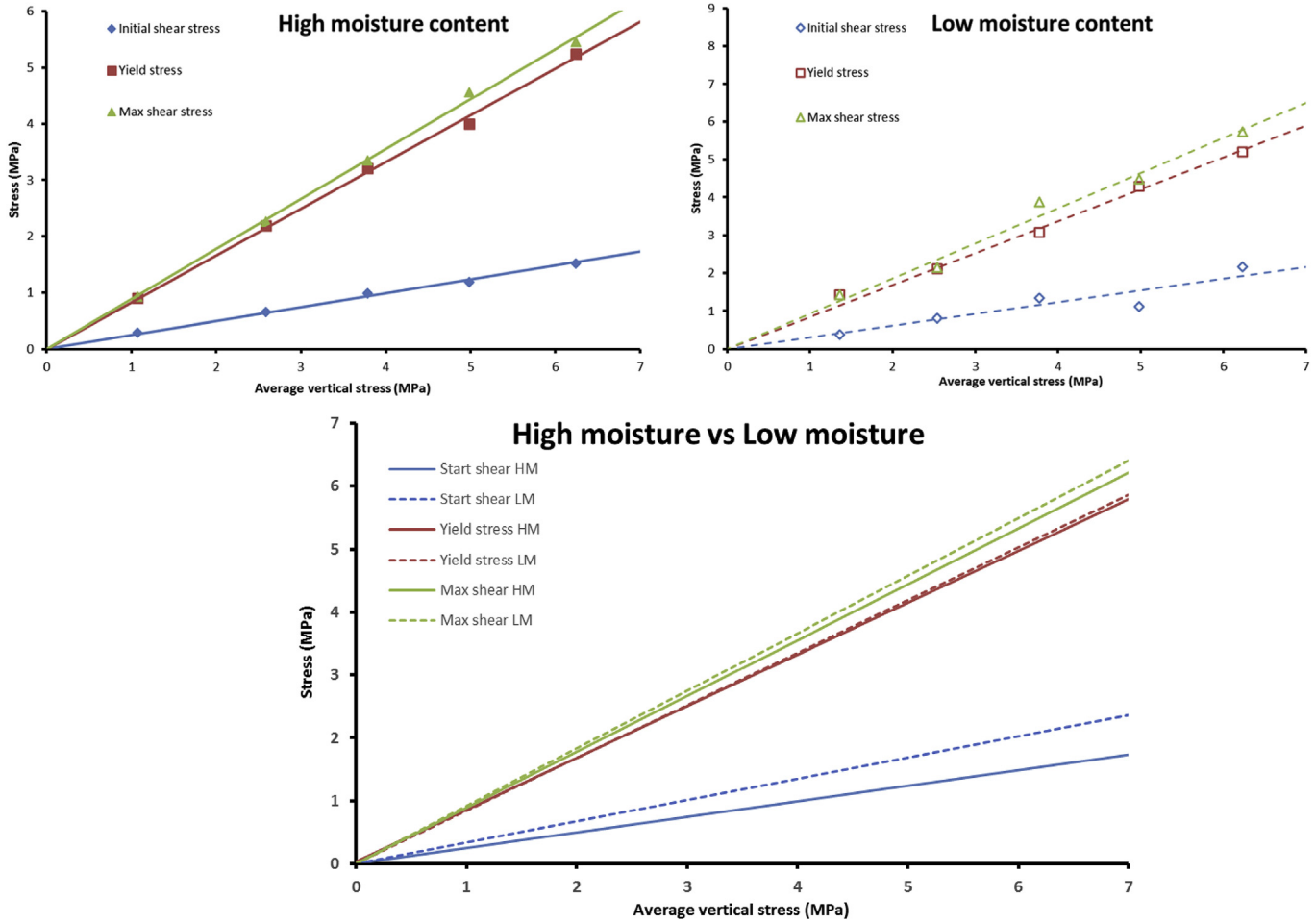


**Fig. 6.** Relationship of shear stress with vertical stress, showing starting shear, yield stress, and maximum shear stress for the higher and lower moisture content gouge. (a) High moisture content tests; (b) low moisture content tests; (c) comparison of high and low moisture content.

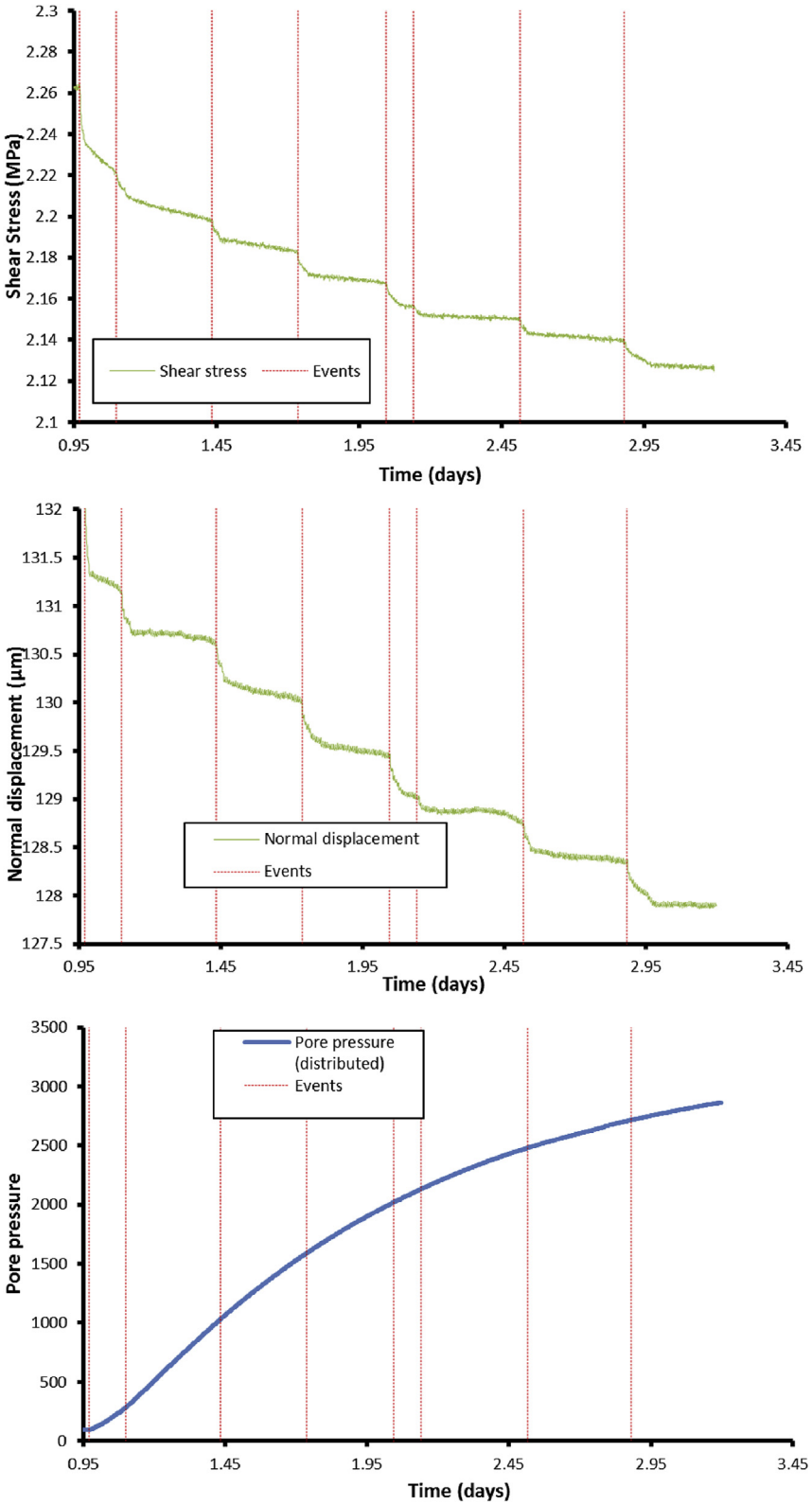


**Fig. 7.** Example of reactivation from Test 3. (a) Shear stress reductions over time, (b) normal displacement reductions over time which coincide with the shear stress events, (c) pore pressure increase during injection phase.

have a slightly higher starting shear stress than the higher moisture content ones. There is less of a difference between the yield and maximum shear stress; however, the lower moisture content tests are slightly above the higher moisture content ones. All of the mechanical data shows a linear relationship with vertical stress.

Once the gouge was critically stressed the second phase of testing could begin. De-ionised water was injected directly onto the fault gouge at a rate of $100\,\mu l\,h^{-1}$, this facilitated the increase of pore pressure within the gouge in an attempt to promote slip. As pore pressure increased, reactivation was noted as a simultaneous drop in the shear

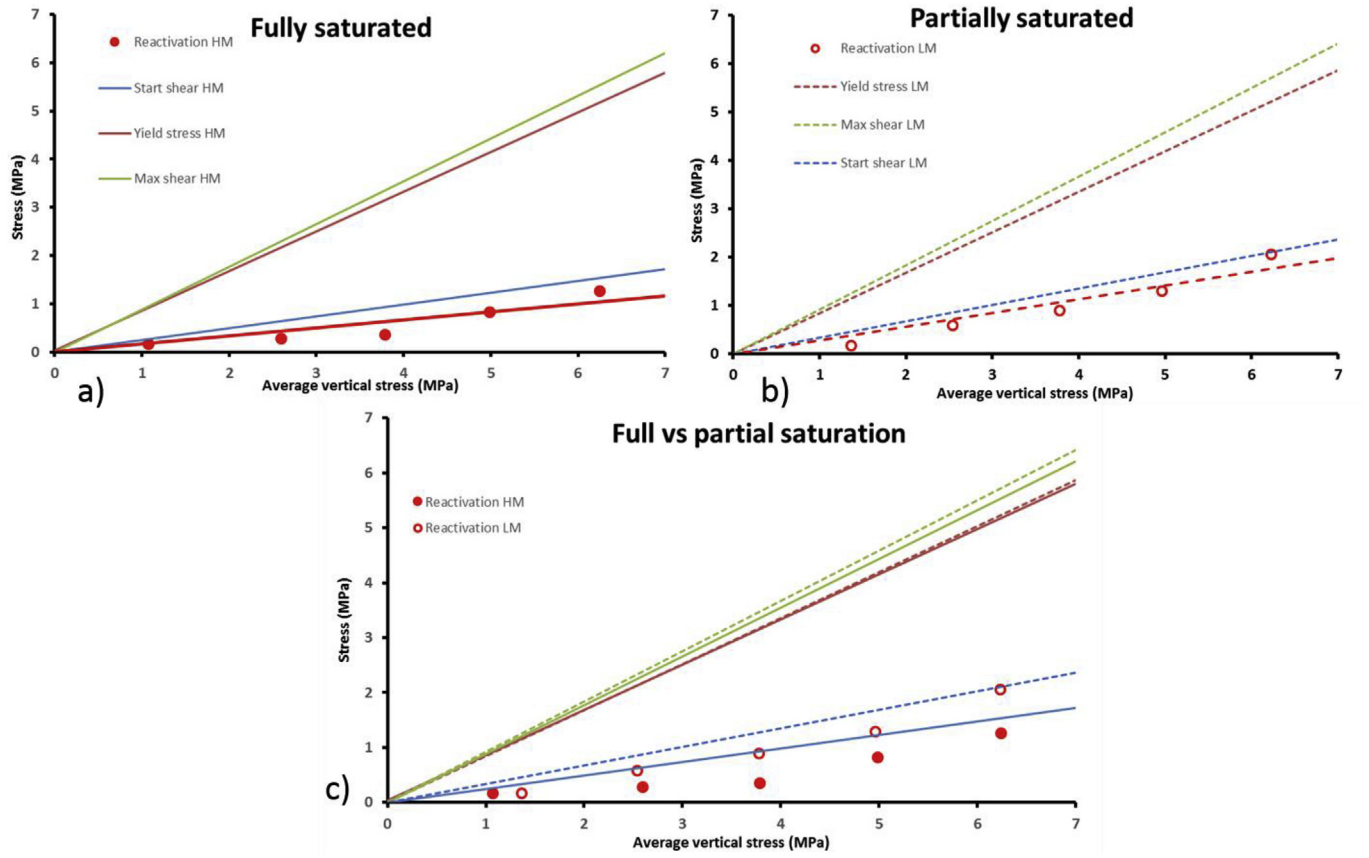


**Fig. 8.** Fault reactivation data for all tests compared with the mechanical response of the fault gouge. (a) high moisture/fully saturated content results; (b) low moisture/partially saturated content results; (c) comparison of high and low moisture results showing the increase in reactivation pressure for the lower moisture content gouge.

stress and vertical displacement. Fig. 7 shows a typical example of observed fault reactivation for Test 3 (2.6 MPa) and the associated pore pressure ramp. The small drops in shear stress (Fig. 7a) and normal displacement (Fig. 7b) were interpreted as fault slip events. The pore pressure was recorded for each of these slip events. The pore pressure is averaged over the whole area of the gouge surface assuming radial flow equating to 0.35 $u$, where $u$ is the injection pore pressure.

As can be seen in Fig. 7, Test 3 reactivated several times as the pore pressure increased. Table 2 presents the first reactivation pressure for each test as well as the number of reactivations that occurred. There is no obvious relationship between the number of reactivations and the vertical stress applied to the gouge; however, each test did slip a minimum of two times.

The pore pressure at the time of the first reactivation in each test is shown against the mechanical data in Fig. 8. Fig. 8a shows that the initial reactivation pressure increases with vertical stress. A similar relationship is observed in Fig. 8b for the partially saturated gouges. In both Fig. 8a and b the reactivation pressure is closely related to the starting shear stress of the gouge. A comparison in reactivation pressures for the separate tests can be seen in Fig. 8c. This shows that the partially saturated gouge reactivated at a higher pore pressure than the fully saturated gouge.

The magnitude of normal displacement and shear stress change is shown in Fig. 9. The magnitude of normal displacement and shear stress changes were calculated using an average of displacement/shear stress value before and after each reactivation event. Fig. 9a and b shows average normal displacement and shear stress change for the reactivation events in each test. The average amount of slip was only calculated for the first three reactivation events as this is the minimum number of reactivation events that occurred during a single test. Fig. 9c and d shows the normal displacement and shear stress changes during the first three reactivation events of each test, to examine how the normal displacement and shear stress changes may evolve over time. It must be noted that all data in Fig. 9 derive from the fully saturated data set, this was chosen due to the higher reliability in the data set, which is described in Fig. 5.

Fig. 9a shows the amount of slip decreased as vertical stress increased. The amount of slip varied from 0.27 to 0.01 μm. A similar relationship with vertical stress is observed in Fig. 9b for the average shear stress change. It must be noted that there is less confidence in the results in Fig. 9b, this is reflected in the lower $R^2$ value. A linear relationship can still be described in both Fig. 9a and b.

Fig. 9c shows the normal displacement for the first three reactivation events in each test. Again, a relationship with the vertical load can be seen, which is a non-linear relationship best described by a negative log relationship. Another clear observation is that subsequent reactivation events slip a greater amount each time. However, the difference is only of the order of a few microns.

Fig. 9d shows the shear stress changes for the first three reactivations. A clear relationship with vertical stress is again seen, this time described best by a second order polynomial. A similar relationship is also seen when comparing the first three reactivations. The lowest shear stress change occurred during the first reactivation and increased for each reactivation event.

## 4. Discussion

This study presents results from a study of fault reactivation in Bowland Shale as a result of pore pressure increase in response to hydraulic stimulation. This test was designed to investigate the controls

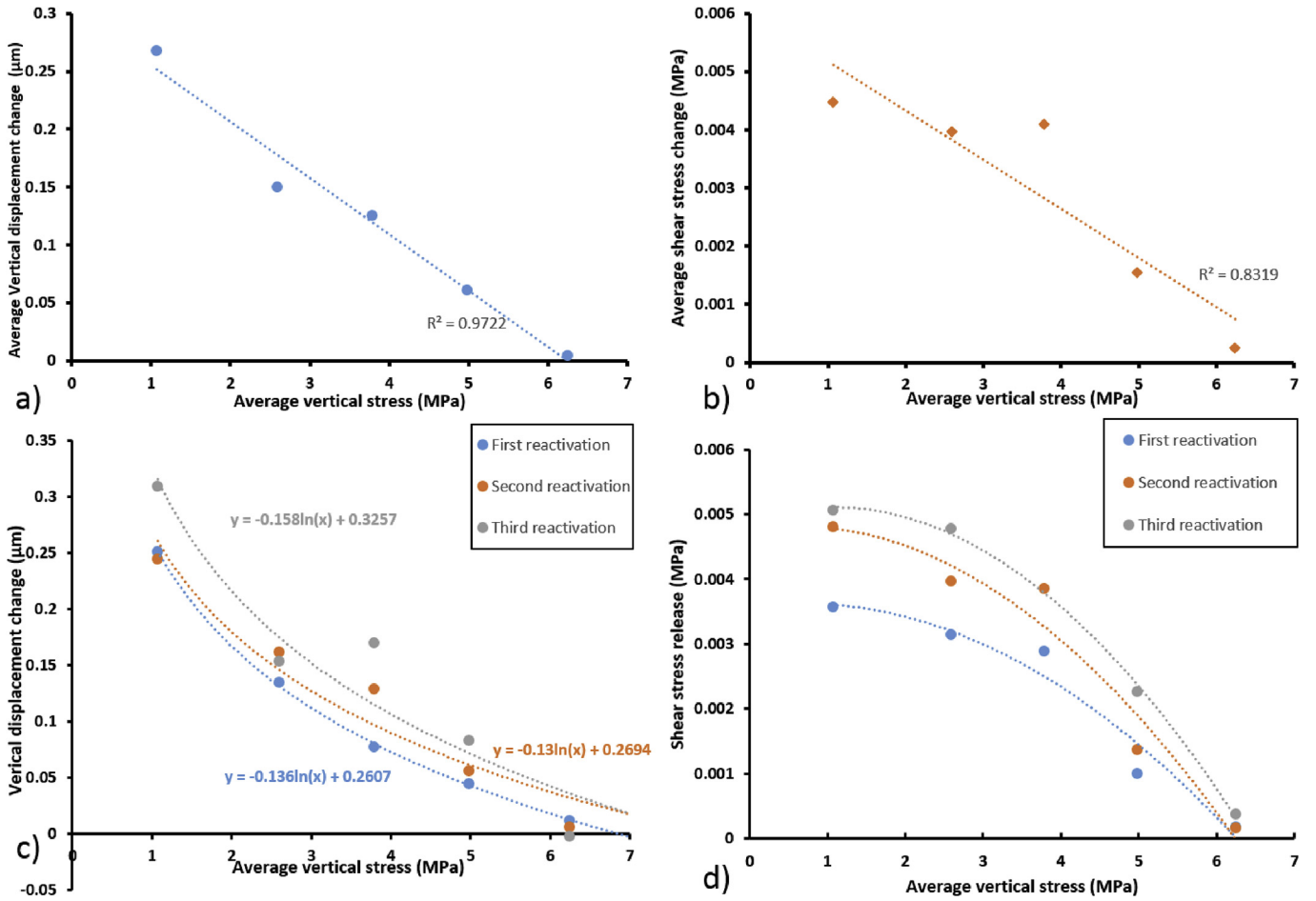


**Fig. 9.** Change in normal displacement and shear stress as a result of fault reactivation. (a) average normal displacement change for each test compared to vertical stress, (b) average shear stress change for each test compared with vertical stress, (c) normal displacement for the first three reactivations of each fully saturated test, (d) shear stress changes for the first three reactivations of each fully saturated test.

on fault slip in Bowland Shale and to replicate conditions of those at Preece Hall and the potential to create felt induced seismicity.

The Bowland Shale used in this study originated in the Pennine Basin, the samples were retrieved from a stream bed exposure at Parlick Hill, Lancashire. Therefore, this rock may not be fully representative of the shale at depth, but in the absence of well-preserved core material this was the best available option. The lack of core material from realistic depths means data is not available to ascertain whether the ball-milled gouge used in this study is representative of fault gouge at depth. The use of gouge was necessary to reduce the number of variables within the experiment by eliminating fracture roughness. Therefore, the experiments are not designed to fully replicate faults at depth but were designed to investigate the controls on fault reactivation based on saturation and mineralogy.

Fig. 5 shows the mechanical responses of the gouge to the initial shearing phase of testing. A good degree of conformity is seen in the mechanical data, especially for the fully saturated case. The starting shear, yield, and maximum shear stress are shown comparatively in Fig. 6. A linear relationship can be seen for each of these mechanical parameters as a function of vertical stress. Therefore there is a clear relationship between strength and depth, meaning faults and fractures will display greater strength at depth. The fully saturated gouge show a good consistency of results, however the same cannot be said for the partially saturated case. The reasons for this are unclear. Sample preparation was carefully conducted to ensure the gouge was as homogeneous as possible. One possible reason for the non-conformity may be shearing of the gouge during setup with a slight rotation of the drive train early in the experiment. Therefore the LVDT was not measuring the true displacement of the fault plane, this may have slightly altered the results in these tests, e.g. Test 14. However, the yield stress of this test conforms with the general trend with depth and therefore only the elastic region of the stress-strain response was affected.

Figs. 5 and 6 also show that there is a slight difference in mechanical strength between the two sets of gouge. The partially saturated gouge has higher starting shear stresses, suggesting the lower moisture content has resulted in a slightly higher cohesive strength. Cohesion is clearly shown as an influence of strength in the Mohr-Coulomb failure criterion (Equation (2)). The yield and maximum shear stress are also slightly higher in the partially-saturated gouge; however, they are still very close and this may be within the error of the measurement.

De Pater and Baisch (2011) discuss a shear and friction study in which the Bowland Shale is found to have relatively weak layers with relatively low shear strength. The Bowland Shale was also found to have a relatively low mechanical strength. This low strength was studied by a series of frictional sliding tests, as described by De Pater and Baisch (2011). They also describe the Bowland Shale as consisting of many faults and fractures. Another finding of this study was that carbonate rich areas had higher strengths than other parts of the sequence, again highlighting the importance of mineralogy on strength. There is therefore some similar findings to the current study.

Table 2 also demonstrates that each test showed evidence for reactivation of the gouge during the injection phase. Fig. 8 shows that the gouge reactivated at pore pressures similar to that of the starting shear stress. The starting shear stress is derived by the translation of the

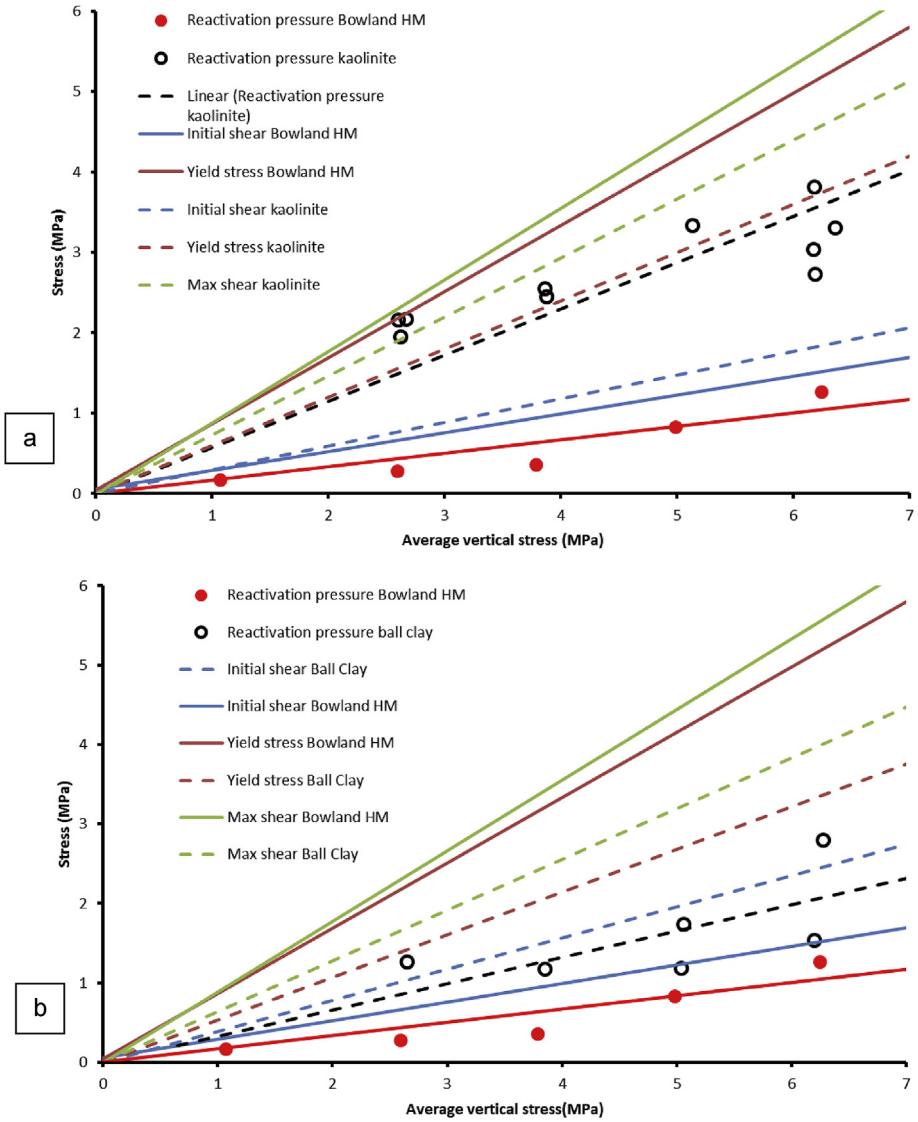


**Fig. 10.** Comparison between high moisture content Bowland Shale and results from Cuss and Harrington (2016) highlighting the importance of mineralogy. (a) comparison between pure kaolinite and Bowland Shale; (b) comparison between Ball Clay and Bowland Shale.

vertical stress into the horizontal plane and is therefore closely related to the Poisson's ratio of the gouge. The saturation state of the gouge is likely to effect the Poisson's ratio and hence result in variations in starting shear stress between the two sets of tests. This in turn means that the reactivation pressure of the gouges is controlled by the Poisson's ratio of the gouge. The gouge has reactivated at relatively low pore pressures, suggesting that the Bowland Shale would make a relatively weak fault gouge.

Table 2 shows the stress conditions which this series of tests were performed. As can be seen, these stress conditions are relatively low when compared to the stresses expected at depths between 2 and 5 km; the expected depths for UK shale gas exploration in the UK (Geol.Soc., 2013). It is possible to extrapolate the stress conditions from this study to those expected. Total vertical stress can be expected to be a minimum of 46 MPa at 2 km depth (assuming 23 MPa $km^{-1}$ stress gradient, Zoback, 2010). Extrapolating the results in Table 2 and the initial reactivation pressures we would expect a fault with the same characteristics as this to reactivate at 7.6 MPa for a fully saturated gouge. Whereas, the partially saturated gouge would reactivate at 15.5 MPa. This further highlights the strengthening factor from the lower moisture content. If we were to then incorporate an effective stress condition, using a 10 MPa $km^{-1}$ hydrostatic gradient, then we would expect reactivation at 4.3 and 8.8 MPa greater than in situ pore pressure for the respective gouge. This upscaling does, however, have many assumptions that would need to be taken into account for more accurate predictions, for example fracture roughness and fracture area.

The normal displacement change during a reactivation event is akin to the amount of slip that has occurred (Fig. 9a,c). Whereas the shear stress change can be related to the amount of energy released during reactivation (Fig. 9b,d). The amount of slip and energy released during these tests is relatively small. However, that is due to the downscaling of the stress conditions and also the size of the fracture. If we were to extend the relationships with depth in Fig. 9 to depths relevant to shale gas (2–5 km; Geol soc., 2013) then the amount of slip would be negligible and the energy released would be sub seismic. It is however, possible to upscale the results of Fig. 9 to a more realistic size fracture. For example, Green et al. (2012) concluded that the Preese Hall seismic event of 2011 occurred over a fracture area of 10,000 $m^2$, which slipped approximately 1 cm. This amount of slip resulted in a $M_L = 2.3$ seismic event. If this energy release was scaled down to a fracture of the size used in this study (0.0036 $m^2$) and a slip distance of 1 μm, then the energy released during our study would be 277 times smaller than that at Preese Hall. This means that when scaled down to the laboratory scale, experiments shown here would be a seismic event with a

magnitude of approximately $M_L = -0.05$. If a seismic event of this magnitude was detected in the UK during a shale gas operation then regular operation would continue according to the traffic light system adopted for seismic monitoring, which was originally recommended by The Royal Society (2012). The differences in this energy release could be due to a number of reasons that these analogue experiments are unable to take account of. For example, scale, mineralogy, stress conditions, and injection rates.

This study aimed to simulate the raising of pore pressure as a result of hydraulic stimulation. However, these experiments are not designed to fully represent every one of the potential variables, therefore some assumptions were made. The variables that we could control were the mineralogy, vertical stress, shear rate, and injection rate. Warpinski et al., 2008 and King (2010) state that the injection rate during hydraulic stimulation is a critical element to be considered in fracture reactivation. Warpinski et al., 2008 observed that injection rates of 15 barrels per minute or less would not trigger microseismic signals, meaning that if reactivation was to occur it would be microseismic. This study used a flow rate of 100 $\mu l\,h^{-1}$ over an extended period of time, whereas during full-scale hydraulic fracturing operations up to half a million gallons of fluid can be pumped over just a few hours (DOE, 2009). This equates to a flow rate of approximately 0.63 $Gl\,h^{-1}$. King (2012) estimated fracture surface areas of between 10,000 and 100,000 $m^2$ as a result of stimulation, meaning that the injection rate equates to 6.3 $l\,h^{-1}\,m^{-2}$. When compared to the current study, equates to a significantly lower rate of 0.03 $l\,h^{-1}\,m^{-2}$; a factor of 150. Therefore, the energy emitted during fracture slip in this study would be expected to be minimal and sub-seismic. Further experiments are therefore needed to examine the amount of energy emitted by fracture reactivation as a function of injection rate.

Another potential control on the strength of a fracture, which is not clear from the current results alone, is the mineralogy of the gouge. In order to gain further insight into this, the current results are compared with previous studies. Cuss and Harrington (2016) performed tests on saturated kaolinite and Ball Clay gouge with the same boundary conditions as the tests in this study (Fig. 10). Again, clear linear relationships were observed for the mechanical data when compared against vertical stress. Fig. 10a compares the results from the fully saturated Bowland Shale gouge with the kaolinite gouge. Kaolinite had a higher starting shear stress, however the yield stress and maximum shear stress are lower than the Bowland Shale. Therefore, the Bowland Shale gouge presents an extended region of elastic deformation when compared with the kaolinite gouge. Fig. 10a also shows the initial reactivation pressures for the kaolinite gouge, which suggests reactivation occurred at a pressure closer to the yield stress, as opposed to reactivation at a pressure close to the starting shear stress.

Fig. 10b shows the results of this study compared with Ball Clay gouge. The Bowland Shale and Ball Clay both show reactivation occurring at pressures close to that of the starting shear stress for the respective gouge. This implies that both the Bowland Shale and Ball Clay gouges are both mechanically weaker than the kaolinite gouge. The starting shear stress closely relates to the cohesion of the material. Cuss and Harrington (2016) showed that the Ball Clay had a cohesion of 0.33 MPa, we would therefore expect the Bowland Shale to have a lower cohesive strength than this due to the mechanical properties shown in Fig. 10b.

The tests in this study were performed at the same boundary conditions as those in Cuss and Harrington (2016) therefore meaning that mineralogy is the clear control on the varying mechanical properties. The kaolinite tests used 100% kaolinite and the Ball Clay had a bulk mineralogy of 37% kaolinite, 35% mica/illite, 26% quartz and small amounts of feldspar (Donohew et al., 2000). Table 1 shows the mineralogy of the Bowland Shale from this study, these were measured using x-ray diffraction techniques. There is clearly a high carbonate content of almost 49% in the Bowland Shale, there is also a relatively high quartz content of 25%. The clay content is relatively low compared to the kaolinite and Ball Clay. The high carbonate and quartz content are likely to be the main controlling factors in the clear mechanical differences. Brittle minerals, such as quartz, have been shown to have a significant effect on the mechanical properties of shale (Jacobi et al., 2008; Rickman et al., 2008; Parker et al., 2009). However, as mentioned above we may expect the Bowland Shale to have a lower cohesive strength than the Ball Clay, therefore meaning the cohesive strength may be the controlling factor on reactivation as opposed to mechanical strength (e.g. yield strength). The varying mineralogical controls on fault strength and potential for reactivation mean that it would be difficult to predict the mechanical strength of a fracture and the pressure at which it would reactivate based purely on mineralogy. However, it is clearly a controlling factor, so the greater the amount of data available on the mineralogy of fracture and fault gouge in the target area for exploration then the more accurate modelling of the reactivation potential can be.

It must be noted that the material used in this study was sourced from a stream bed cutting and will therefore have been subject to weathering and hydraulic processes. Thus, meaning the mineralogy may not be fully representative of the Upper Bowland Shale at reservoir depth. However, as stated, due to a lack of high quality core material this material is as representative as possible. Furthermore, shale is a very heterogeneous material and can vary significantly over short distances (Cuss et al., 2015), therefore this data cannot be applied to the whole of the Upper Bowland Shale. Further study is needed to examine the mineralogy of fractures and fault gouge in the Bowland Shale. For this to occur high quality, well preserved core material is required.

Cuss and Harrington (2016) showed that reactivation pressure showed a single linear relationship for kaolinite and Ball Clay when plotted in the effective mean stress [$P = {}^1/_3(\sigma_1 + \sigma_2 + \sigma_3) - P_p$] versus differential stress [$Q = \sigma_3 - \sigma_1$] space. Whilst that study only looked at two clay gouges, it was suggested that different clay gouges would behave similarly. Fig. 11 shows the current data plotted with the data of Cuss and Harrington (2016). This clearly shows that a single relationship does not exist and that Bowland Shale shows a considerable reduction in differential stress at reactivation, mainly as a result of a low pore pressure at reactivation.

The data shown in Fig. 11a suggests that a single slope of reactivation pressure may exist in the Q-P space, with variations in intercept. A macro was written in Microsoft Excel to adjust the intercept of Ball Clay and Bowland Shale to create a unified relationship relative to kaolinite, as shown in Fig. 11b. Although spread of the data about the general trend is considerable, a unified relationship has been achieved with a single slope of 0.412 and an $R^2$ of 0.82. Fig. 11c shows the current data and that of Cuss and Harrington (2016) plotted with the best fit for a slope of 0.412. This suggests that Ball Clay has an offset incept of 0.28 MPa compared with kaolinite. For fully saturated Bowland Shale an offset of 1.5 MPa is observed, with 1.23 MPa seen for Bowland Shale with a reduced water content. This suggests that the reduction in kaolinite content from 100% to 37% for Ball Clay, in addition to 35% mica/illite and 26% quartz, reduces the strength of faults by 0.28 MPa. Further, the mineralogy of the Bowland Shale reduces the strength of faults by 1.5 MPa.

Close inspection of the fit of the slope of 0.412 to the Bowland Shale shows a poor fit for full saturation. Therefore, Bowland Shale has been investigated as having a different slope, but with a common slope for the two saturation states tested, as shown in Fig. 12. In this case, kaolinite and Ball Clay have a common slope of 0.52, while Bowland Shale has a slope of 0.22. This gives a much improved fit to the data for each gouge type and may represent differences in frictional properties of the gouges investigated. This shows that Ball Clay has a reduced strength of 0.46 MPa, while Bowland Shale has a reduced strength of 0.85 MPa. In addition, with increasing mean stress (i.e. depth) Bowland Shale cannot sustain as much pore pressure at fault reactivation, and thus appears weaker.

More data is needed to determine whether clay gouge of different

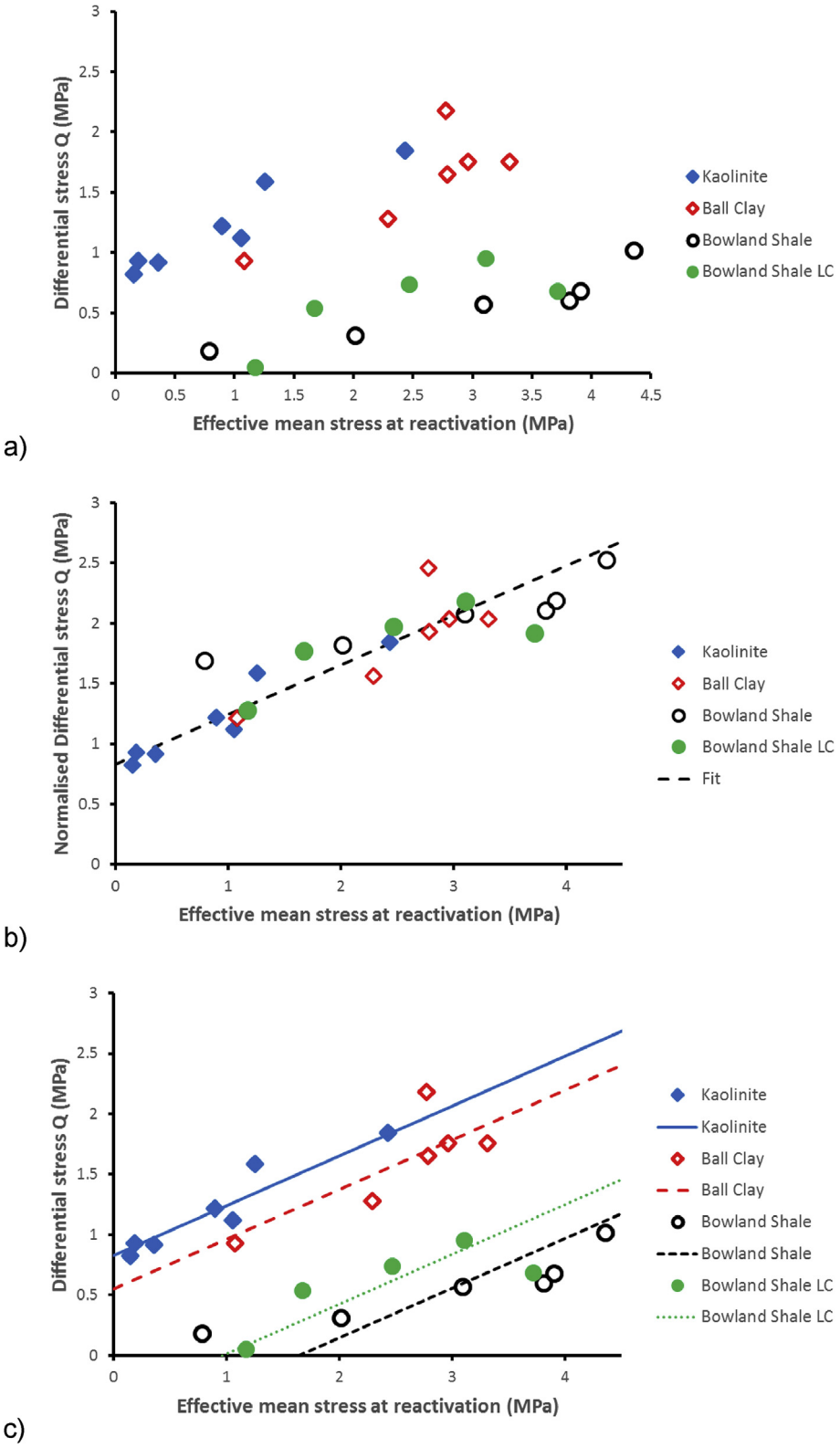


**Fig. 11.** Fault reactivation envelopes in the effective mean stress versus differential stress space. a) Data from the current study for Bowland Shale and from Cuss and Harrington (2016); b) a unified relationship for clay gouge; c) unified slope fit to all four clay gouges.

mineralogy conform to a single slope, or multiple slopes. However, we can still conclude that mineralogy has a strong influence on fault re-activation. The tests in this study and those of Cuss and Harrington (2016) were performed in a similar manner, using the same apparatus and under similar stress conditions. Therefore, the only variable is the gouge mineralogy and the associated change in properties this brings with it.

The current data, and that of Cuss and Harrington (2016) were all achieved by raising the pore pressure on a critically stressed fault,.i.e. at peak strength conditions of the gouge. Cuss et al. (2016) showed that a

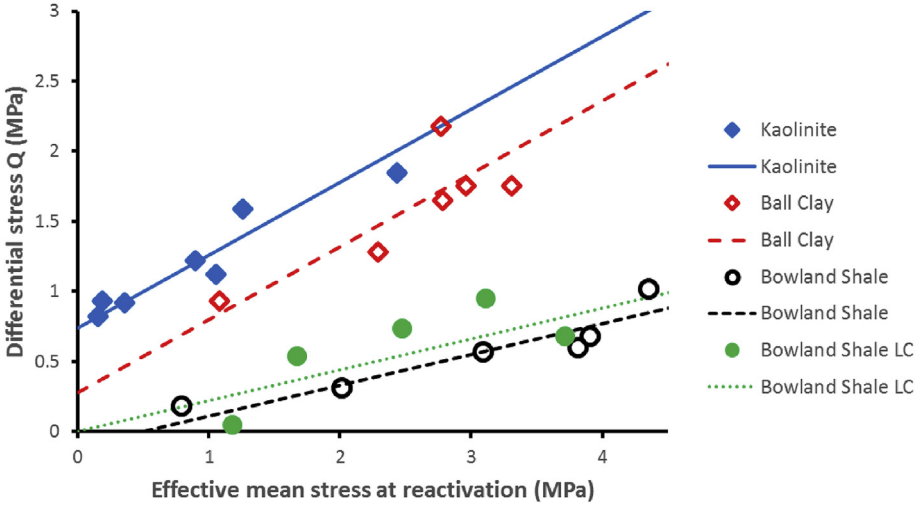


**Fig. 12.** Fault reactivation envelopes in the effective mean stress versus differential stress space. A unified slope has been assumed for kaolinite and Ball Clay, with a separate slope for the two Bowland Shale clay gouge.

reduction in the vertical stress resulted in a stress memory by the fault, i.e. the strength remained at that achieved at the maximum stress condition. Thus meaning, that along with mineralogy and saturation state, the stress history of a fault or fracture can be a control on mechanical strength and subsequently effect the reactivation conditions. This is therefore another factor that must be taken into account during exploration. However, it must be noted that the stress conditions in this study and those of Cuss and Harrington (2016) were relatively low and therefore further experiments are required to understand this process at depths more closely related to that of the shale gas industry.

## 5. Conclusions and further work

The fault reactivation properties of a Bowland Shale fault gouge were investigated in this study. The scenario of interest was the raising of pore pressure on a critically stressed fault as a result of hydraulic stimulation. It is important to understand the controls on the mechanical and reactivation properties of faults in order to understand how pore pressure variations will affect pre-existing fracture and faults. Changes in pore pressure can have a key impact on potential hydrocarbon outputs and the environmental impact if large faults become reactivated. The results show that there are a number of key controls on fracture reactivation, many of which need further investigation.

Using a Bowland Shale gouge, which was shown to have a high carbonate content, we have defined the mechanical and reactivation properties of the gouge. When comparing these results to tests on other mineralogy gouges we see that the results are not similar. Therefore showing mineralogy to be a key control on fault properties. The Bowland Shale was also shown to be a relatively weak fault gouge under the pressure conditions used in this study.

Two sets of tests were performed in this study; one on a fully saturated gouge and another on a lesser saturated gouge. It is clear from the mechanical results that decreasing water content had a positive influence on the strength of the gouge. This had a consequence on the reactivation properties as the lesser saturated gouge reactivated at slightly higher pore pressures. Therefore, saturation state of a fault gouge is one of a number of controls on both mechanical strength and reactivation pressure.

Results in this study show that reactivation can occur several times on the same fault. The slip and energy release associated with each reactivation is complex. For the fully saturated gouge the energy released increased after each event for the first three reactivations. However, the less saturated gouge was much more complex and therefore difficult to interpret a pattern.

This study has shown that in order to gain a more detailed view on the potential for fault reactivation as a result of pore pressure increase during hydraulic stimulation a knowledge of the gouge mineralogy and saturation state is necessary. In addition, an estimate of fault orientation, in situ stresses (including pore pressure), stress history, and operational pressure regimes are required. Further experimental work can look at a greater number of variables e.g. fluid pressurisation rate, fluid composition, and liquid absorption. It is clear that even in idealised analogue faults with well constrained boundary conditions, fault reactivation is a complex phenomena. This research will benefit from investigations on the reactivation properties of competent shale samples. This will help aid in bridging the gap between analogue tests, such as this study, and the field scale.

## Acknowledgements

This study was undertaken by staff of the Minerals and Waste Programme and the Energy & Marine Geoscience Programme at the British Geological Survey. Funding for this study was provided by the European Union's Horizon 2020 Research and Innovation Programme (grant agreement number 640715) as part of the M4ShaleGas Project; Measuring, Monitoring, mitigating and managing the environmental impact of shale gas.

This paper is published with the permission of the Executive Director, British Geological Survey (NERC).

## References

Andrews, I.J., 2013. The Carboniferous Bowland Shale Gas Study: Geology and Resource Estimation. British Geological Survey for Department of Energy and Climate Change, London, UK.

API, 2009. Hydraulic Fracturing Operations: Well Construction and Integrity Guidelines. API Guidance Document HF1. American Petroleum Institute, Washington, DC.

Arthur, J.D., Bohm, B., Coughlin, B.J., Layne, M., 2008. Evaluating the Environmental Implications of Hydraulic Fracturing in Shale Gas Reservoirs. ALL Consulting, Tulsa, OK.

Boozer, G.D., Hiller, K.H., Serdengecti, S., 1963. Effects of pore fluids on the deformation behaviour of rocks subjected to triaxial compression. In: Fairhurst, C. (Ed.), Rock Mechanics, 5th Symosium of Rock Mechanics. Oxford Pergamon press, pp. 579–624.

Clarke, H., Eisner, L., Styles, P., Turner, P., 2014. Felt Seismicity Associated with Shale Gas Hydraulic Fracturing: the First Documented Example in Europe. Goephysical Research Letters. https://doi.org/10.1002/2014GL062047.

Cuss, R., 1999. An Experimental Investigation of the Mechanical Behaviour of Sandstones with Reference to Borehole Stability. Ph.D. Thesis. The University of Manchester.

Cuss, R.J., Harrington, J.F., 2016. An experimental study of the potential for fault reactivation during changes in gas and porewater pressure. International Journal of Greenhouse Gas Control 53, 41–55. https://doi.org/10.1016/j.ijggc.2016.07.028.

Cuss, R.J., Milodowski, A.E., Harrington, J.F., Noy, D.J., 2009. Fracture Transmissivity Test of an Idealised Fracture in Opalinus Clay. British Geological Survey

Commissioned Report, pp. 74 CR-09/163.
Cuss, R.J., Milodowski, A., Harrington, J.F., 2011. Fracture transmissivity as a function of normal and shear stress: first results in Opalinus Clay. Phys. Chem. Earth, Parts A/B/C 36, 1960–1971.
Cuss, R.J., Wiseall, A.C., Hennissen, J.A.I., Waters, C.N., Kemp, S.J., Ougier-Simonin, A., Holyoake, S., Haslam, R.B., 2015. Hydraulic Fracturing: a Review of Theory and Field Experience. M4ShaleGas Report D1.1, British Geological Survey, Nottingham, United Kingdom. The M4ShaleGas Project Is Funded by the European Union's Horizon 2020 Research and Innovation Programme under grant Agreement Number 640715. . www.m4shalegas.eu.
Cuss, R.J., Graham, C.C., Wiseall, A.C., Harrington, J.F., 2016. Cyclic loading of an idealized clay-filled fault; comparing hydraulic flow in two clay gouges. Geofluids 16, 552–564. https://doi.org/10.1111/gfl.12175.
Cuss, R.J., Wiseall, A.C., Tamayo-Mas, E., Harrington, J.F., 2018. An experimental study of the influence of stress history on fault slip during injection of supercritical CO2. J. Struct. Geol. 109, 86–98.
Davies, R.J., Mathias, S.A., Moss, J., Hustoft, S., Newport, L., 2012. Hydraulic fractures: how far can they go? Mar. Petrol. Geol. 26, 1–6.
De Pater, C.J., Baisch, S., 2011. Geomechanical Study of Bowland Shale Seismicity. StrataGen Report for Cuadrilla, Synthesis Report 57.
DOE, Prepared by Ground Water Protection Council and ALL Consulting, 2009. Modern Shale Gas Development in the United States: a Primer. US Department of Energy, Office of Fossil Energy and National Energy Technology Laboratory, Washington DC.
Donohew, A.T., Horseman, S.T., Harrington, J.F., 2000. Gas entry into unconfined clay pastes at water contents between the liquid and plastic limits. In: Cotter-Howells, J.D., Campbell, L.S., Valsami-Jones, E., Batchelder, M. (Eds.), Environmental Mineralogy: Microbial Interactions, Anthropogenic Influences, Contaminated Land and Waste Management. Mineralogical Society Series 9, Mineralogical Society, London, 0 903056 20 8, pp. 369–394.
Dyke, C.G., Dobereiner, L., 1991. Evaluating the strength and deformability of sandstones. Q. J. Eng. Geol. 24, 123–134.
EIA, U.S. Energy Information Administration, 2016. 2016 International Energy Outlook 2016. DOE/EIA-0484.
EU, 2011. Energy Roadmap 2050. European Commission 885 final of , Accessed date: 15 December 2011.
Fisher, K., Warpinski, N.R., 2012. Hydraulic-fracture-height Growth: Real Data. Society of Petroleum Engineershttps://doi.org/10.2118/145949-PA.
Gale, J., Holder, J., 2008. Natural fractures in the Barnett Shale: constraints on spatial organization and tensile strength with implications for hydraulic fracture treatment in shale-gas reservoirs. In: Proceedings of the 42nd US Rock Mechanics Symposium.
Gale, J.F., Reed, R.M., Holder, J., 2007. Natural fractures in the Barnett Shale and their importance for hydraulic fracture treatments. AAPG (Am. Assoc. Pet. Geol.) Bull. 603–622.
Gale, J.F., Laubach, S.E., Olson, J.E., Eichbul, P., Fall, A., 2014. Natural fractures in shale: a review and new observations. AAPG (Am. Assoc. Pet. Geol.) Bull. 11, 2165–2216.
Geol Soc, 2013. Shale Gas: Challenges and Opportunities. A briefing note by the Geological Society of London, UK, pp. 4.
Green, C.A., Styles, P., Baptie, B., 2012. Preese Hall Shale Gas Fracturing: Review and Recommendations for Induced Seismic Mitigation. (DECC commissioned report).
Hawkins, A.B., McConnell, B.J., 1992. Sensitivity of sandstone strength and deformability to changes in moisture content. Q. J. Eng. Geol. 25, 115–130.
Hubbert, M.K., Rubey, W.W., 1959. Role of fluid pressure in mechanics of overthrusting faulting: mechanics of fluid-filled porous solids and its application to overthrusting faulting. Geol. Soc. Am. Bull. 70, 115–166.
Ikari, M.J., Saffer, D.M., Marone, C., 2007. Effect of hydration state on the frictional properties of montmorillonite-based fault gouge. J. Geophys. Res. 112, B06423. https://doi.org/10.1029/2006JB004748.
Jacobi, D., Breig, J., LeCompte, B., Kopal, M., Hursan, G., Mendez, F., Bliven, S., Longo, J., 2008. Effective geomechanical and geochemical characterisation of shale gas reservoirs from the wellbore environment: caney and the Woodford Shales. In: SPE Annual Technical Conference and Exhibition. Society of Petroleum Engineers.
King, G.E., 2010. Thirty Years of Gas Shale Fracturing: what Have We Learned? Society of Petroleum Engineers.
King, G.E., 2012. Hydraulic Fracturing 101: what Every Representative, Environmentalist, Regulator, Reporter, Investor, university Researcher, Neighbours and Engineer Should Know about Estimating Frac Risk and Improving Frac Performance in Unconventional Gas and Oil wells. Society of Petroleum Engineers. Hydraulic Fracturing Technology, Woodlands, TX 2012.
Konitzer, S.F., Davies, S.J., Stephenson, M.H., Leng, M.J., 2014. Depositional controls on mudstone lithofacies in a basinal setting: implications for the delivery of sediment and organic matter. J. Sediment. Res. 84, 198–214.
Mair, R., m Bickle, M., Goodman, D., Koppelman, B., Roberts, J., Selley, R., Shipton, Z., Thomas, H., Walker, A., Woods, E., Younger, P.L., 2012. Shale Gas Extraction in the UK: a Review of Hydraulic Fracturing. Royal Society and Royal Academy of Engineering, London, pp. 76.
Maxwell, S.C., Watlmann, C.L., Warpinski, N.R., Mayerhofer, M.J., Boroumand, N., 2006. Imaging Seismic Deformation Induce by Hydraulic Fracture Complexity. SPE 102801.
Montogomery, S.L., Jarvie, D., Bowker, K., Pollastro, R.M., 2005. Mississippian Barnett Shale, Fort Worth basin, north-central Texas: gas-shale play with multi-trillion cubic foot potential. AAPG (Am. Assoc. Pet. Geol.) Bull. 89, 155–175.
Ougier-Simonin, A., Renard, F., Boehm, C., Vidal-Gilbert, S., 2016. Microfracturing and microporosity in shales. Earth Sci. Rev. 162, 198–226.
Parker, M., Buller, D., Petre, E., Dreher, D., 2009. Haynesville Shale—petrophysical Evaluation. SPE122937, 11.
Paterson, M.S., 1978. Experimental Rock Deformation – the Brittle Field. Springer-Verlag, Berlin.
Rickman, R., Mullen, M., Petre, E., Greiser, W., Kundert, D., 2008. A practical use of shale petrophysics for stimulation design optimization: all shale plays are not clones of the Barnett Shale. SPE 115258, 11.
Rutqvist, J., Rinaldi, A.P., Cappa, F., Moridis, G.J., 2013. Modeling of fault reactivation and induced seismicity during hydraulic fracturing of shale-gas reservoirs. J. Petrol. Sci. Eng. 107, 31–44.
Rutter, E.H., 1972. An Experimental Study of the Factors Affecting the Rheological Properties of Rock in Simulated Geological Environments. Unpublished Ph.D. Thesis. University of London.
Serdengecti, S., Boozer, G.D., 1961. The effects of strain rate and temperature on the behavior of rocks subjected to triaxial compression. In: Hartman, H.L. (Ed.), Proc. 4th Symp. Rock Mechanics. 76. Penn. State Univ., Bull. Min. Ind. Exp. Sta, pp. 83–97.
Terzaghi, K., 1943. Theoretical Soil Mechanics. Wiley.
The Royal Society and The Royal Academy of Engineering, 2012. Shale Gas Extraction in the UK: a Review of Hydraulic Fracturing. DES2597.
Warpinski, N.R., Mayerhofer, M.J., Vincent, M.C., Cipolla, C.L., Lolon, E.P., 2008. Stimulating unconventional reservoirs: maximizing network growth while optimizing fracture conductivity. J. Can. Petrol. Technol. 48 (10), 39–51.
Zhu, W., Wong, T.-F., 1997. Shear enhanced compaction in sandstone under nominally dry and water-saturated conditions. International Journal of Rock Mechanics and Minerals Science 34.
Zoback, M.D., 2010. Reservoir Geomechanics. Cambridge University Press, pp. 449.